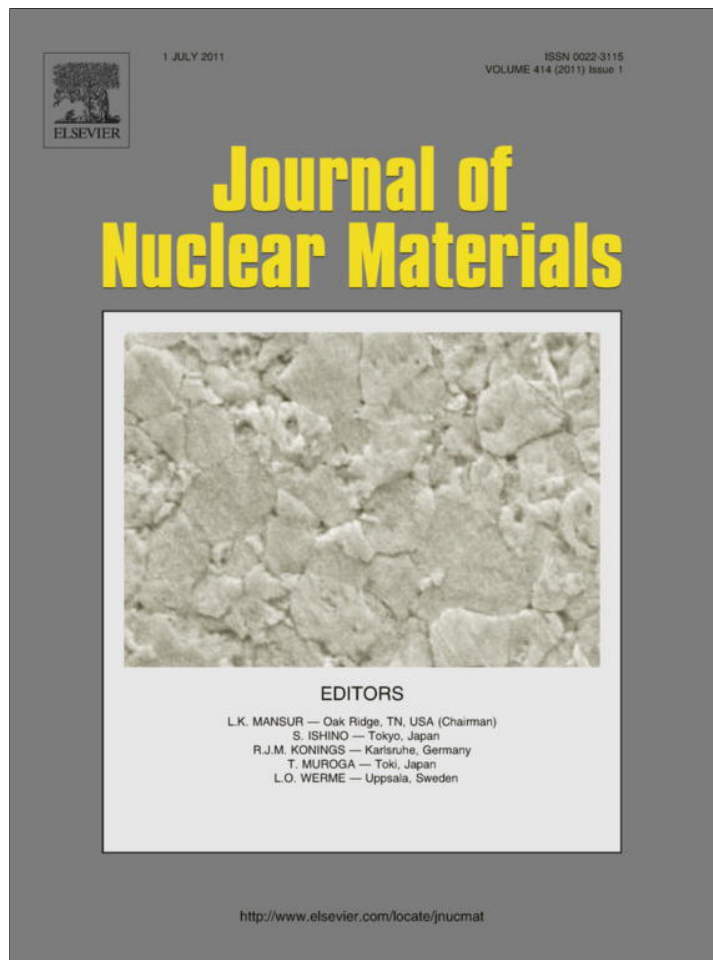


Provided for non-commercial research and education use.  
Not for reproduction, distribution or commercial use.



This article appeared in a journal published by Elsevier. The attached copy is furnished to the author for internal non-commercial research and education use, including for instruction at the authors institution and sharing with colleagues.

Other uses, including reproduction and distribution, or selling or licensing copies, or posting to personal, institutional or third party websites are prohibited.

In most cases authors are permitted to post their version of the article (e.g. in Word or Tex form) to their personal website or institutional repository. Authors requiring further information regarding Elsevier's archiving and manuscript policies are encouraged to visit:

<http://www.elsevier.com/copyright>



Contents lists available at ScienceDirect

## Journal of Nuclear Materials

journal homepage: [www.elsevier.com/locate/jnucmat](http://www.elsevier.com/locate/jnucmat)

## Modelling the erosion of beryllium carbide surfaces

M. Mehine<sup>a,\*</sup>, C. Björkas<sup>a</sup>, K. Vörtler<sup>a</sup>, K. Nordlund<sup>a</sup>, M.I. Airila<sup>b</sup><sup>a</sup> Association EURATOM-Tekes Department of Physics, University of Helsinki, P.O. Box 43, FI-00014, Finland<sup>b</sup> Association EURATOM-Tekes, VTT Technical Research Centre of Finland, P.O. Box 1000, FI-02044 VTT, Finland

## ARTICLE INFO

## Article history:

Received 17 November 2010

Accepted 19 March 2011

Available online 29 March 2011

## ABSTRACT

Redeposition of beryllium eroded from main chamber plasma facing components of ITER onto the divertor material carbon creates a mixed material, beryllium carbide Be<sub>2</sub>C, whose interaction with the plasma is not well known. In this study, we have investigated the erosion of Be<sub>2</sub>C by deuterium using molecular dynamics simulations and ERO impurity modelling. We found that beryllium sputters preferentially over carbon and identified the sputtering mechanism in the ion energy range 10–100 eV to be both physical and swift chemical sputtering. In addition to single atoms, different types of small molecules/clusters were sputtered, the most frequently occurring molecules being BeD, Be<sub>2</sub>D, and CD. The sputtering threshold was found to lie between 10 and 15 eV. The MD sputtering yields were used in plasma impurity simulations, serving as a replacement for input data obtained with TRIM. This changes the accumulation rate of impurity Be in the divertor region compared to previous estimates.

© 2011 Elsevier B.V. All rights reserved.

## 1. Introduction

A current concern in fusion reactors is erosion of wall materials, which leads to contamination of the fusion plasma and limits the lifetime of the first wall. Low energy hydrogen isotopes escaping the fusion plasma have a strong impact on the walls of a fusion reactor. The interplay between the particles and wall materials is commonly named “plasma-wall interactions” (PWI) and will crucially contribute to the degradation of the reactor performance. PWI lead to sputtering erosion, redeposition, tritium retention, and the formation of “plasma-altered materials”, so called mixed materials [1–3]. In this context the sputtered species will harm the plasma. The creation of a mixed material layer is noteworthy since its properties can substantially differ from those of its constituents [2].

The current wall material choice for the next generation experimental fusion reactor ITER [4] is beryllium, carbon, and tungsten [5], hence, mixed layers of these materials are expected. The rate, location and extent of the creation of mixed layers are by no means fully known, nor is the sputtering of these materials. Carbide formation on beryllium surfaces has, however, been observed to mitigate not only the pure beryllium but also the pure carbon sputtering yields [6,7].

One of the main applications of the present work is modelling of impurity migration in fusion plasmas. For local impurity modelling the leading European code is ERO [8,9] – a 3D Monte Carlo impurity transport code that has been applied to several limiter and

divertor tokamaks as well as linear plasma experiments, see, e.g., [10–15]. ERO depends crucially on high-quality data for PWI as well as for dissociation, ionization and emission data for impurities in the plasma. Molecular dynamics (MD) data improve the modelling capability of ERO by providing a more accurate description of low-energy sputtering compared to the data set [16] based on TRIM calculations.

As an attempt to gain an atomic level insight into the sputtering process of Be<sub>2</sub>C, we simulate cumulative bombardment of D on Be<sub>2</sub>C surfaces using MD. The resulting sputtering yields are applied to ITER plasma impurity modelling using ERO. Furthermore, new in this study is the investigation of the mixed material Be<sub>2</sub>C sputtering mechanism at energies up to 100 eV. Also, the materials sputtering yields at low fluences are simulated. Sputtering at higher energies (bombardment energies greater than 100 eV) is relatively well understood and hence we investigate energies near the sputtering threshold. In experiment the actual distribution of impact angles cannot be easily determined – especially in the case of rough surfaces – but it is often assumed that the angle-averaged sputtering yield is twice the yield for normal incidence. Therefore the MD simulations are limited to incidence bombardment.

## 2. Methods

## 2.1. MD simulations

MD is typically very well suited for systems containing up to several tens of millions of atoms and for timescales under 1 nano-second. However, performing cumulative simulations, considerable parallelization is not feasible, hence, our sputtering simulations are

\* Corresponding author.

E-mail address: [mooses.mehine@helsinki.fi](mailto:mooses.mehine@helsinki.fi) (M. Mehine).

limited to systems of a few thousands of atoms. This obviously does not correspond to the scale of a fusion reactor wall, but it can be considered a representative part of the wall and gives valuable insight into the microscopic phenomena plasma-wall interaction.

In this work, the simulations were performed with the PARCAS molecular dynamics code [17]. The potential describing the deuterium, beryllium, and carbon interatomic interactions, including bond breaking and forming, was recently developed by our group [18].

For our simulations, we constructed beryllium carbide antifluorite cells with the dimensions of  $27.5 \times 27.5 \times 45.7 \text{ \AA}$  (consisting of  $6 \times 6 \times 10$  unit cells with a total of 4320 atoms). The cells were initially relaxed at 300 K using Berendsen temperature control [19]. In order to mimic the cell being a small part of the fusion reactor wall we used the  $x$  and  $y$  directions as periodic boundaries as well as fixed the two bottommost layers of the cell in the  $z$  direction. Initial cells having either a beryllium or a carbon terminated surface were constructed.

We bombarded the initial cells cumulatively with deuterium ions where all projectiles had the same initial energy, either 10, 15, 20, 50, 75 or 100 eV. We performed up to 4000 bombardments for each energy and both C or Be terminated surfaces were used.

The impact point of the bombarding deuterium ion was randomized by shifting the cell in the  $x$  and  $y$  direction after every run while keeping the deuterium starting position at the beginning of the simulation in the middle of the  $xy$ -plane and  $5 \text{ \AA}$  above the cell surface. The impact angle of the ion was normal to the surface.

Furthermore, the temperature of the border of the cell was kept at 300 K during the beginning of each bombardment and after 4 ps the whole cell was quenched to 300 K at a rate of  $0.1 \text{ K/fs}$  for 3 ps. One single bombardment simulation lasted 7 ps, thus creating a high flux of  $1.88 \times 10^{28} \text{ m}^{-2} \text{ s}^{-1}$  compared to the expected fluxes in ITER's divertor being of the order of  $10^{24} \text{ m}^{-2} \text{ s}^{-1}$  [5]. Our simulations reached fluences up to  $5.28 \times 10^{20} \text{ m}^{-2}$  which is much lower than typical fluences of one 400-second-long ITER pulse, about  $10^{26} \text{ m}^{-2}$  [5].

The collisions of atoms with electrons cause the ions to slow down when entering the bulk. This damping was taken into account by adding a frictional force depending on the speed of the moving particle. The ZBL electronic stopping [20] was applied to atoms with an energy above 1 eV, not including incoming D ions or sputtered species.

We defined an atom or a molecule/cluster to be sputtered when it was no longer bonded to the surface of the cell. The sputtering yields were gained by averaging the number of eroded atoms over the number of ion impacts. The  $1\sigma$  standard error of the average was calculated.

## 2.2. ERO simulations

Sputtering data for  $\text{Be}_2\text{C}$  cannot be directly used in the so-called homogeneous material mixing (HMM) surface model of ERO. The model is based on the assumption that all substrate and impurity materials mixing takes place in an interaction layer of user-defined thickness. The concentrations of various atom species in the interaction layer of each surface cell evolve during the simulation. At any time moment, sputtering yields, and reflection probabilities are calculated as concentration-weighted averages from the data for pure elements. We modified the surface model so that data for  $\text{Be}_2\text{C}$  – and later for other compounds/mixtures in the ITER-relevant Be/W/C system – can be added as intermediate data points for interpolation between Be and C (and W). This approach can be motivated by the experimental observation that complex binary phase diagrams for compounds with intermetallic phases frequently can be interpreted as combinations of simpler phase diagrams between the pure elements and intermetallic phases

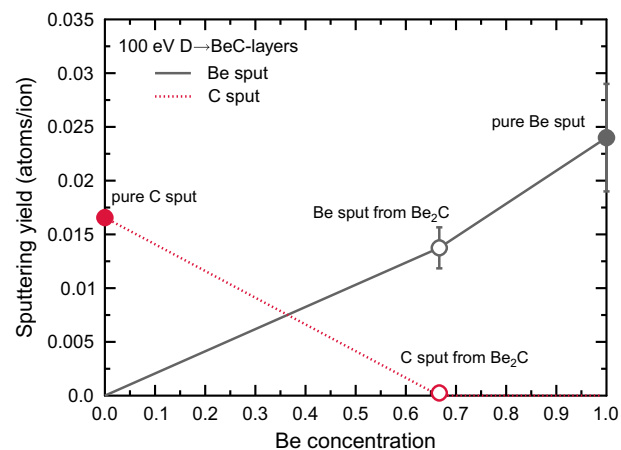


**Fig. 1.** The elemental sputtering yield for surface layers of different concentration. The point for  $\text{Be}_2\text{C}$  is obtained in this work (using the Be terminated surface data), and linear interpolations to the pure C sputtering (TRIM.SP data) and pure Be sputtering [23] are done.

[21,22]. In the model we assume that the maximum stoichiometrically possible amount of  $\text{Be}_2\text{C}$  is formed. Then the data interpolation is done between  $\text{Be}_2\text{C}$  and the remaining Be or C. Fig. 1 illustrates this approach for 100 eV incoming deuterium ions.

We demonstrate the use and significance of the new data set by applying the data to the ITER tritium retention and target lifetime calculation reported in [13]. In this reference case simultaneous erosion of CFC divertor targets and beryllium deposition from the plasma has been estimated using ERO simulations. Due to the main wall erosion, it is assumed that the deuterium plasma flowing onto the divertor targets contains 0.1% beryllium. To separate the effects of new data for beryllium self sputtering (from Ref. [18]) and the description for  $\text{Be}_2\text{C}$  formation, we applied them both separately and together to the reference case. Only using the pure beryllium data is denoted “case 1” and the  $\text{Be}_2\text{C}$  model is “case 2”.

## 3. Results and discussion

### 3.1. MD sputtering yields

Table 1 shows the total number of sputtered atoms as well as every type of molecules that were sputtered in the D on  $\text{Be}_2\text{C}$  simulations. As seen, there was a significant amount of both sputtered Be and C atoms at energies near to 100 eV. The BeD sputtering is noteworthy, and these molecules have been observed in D plasma sputtering experiment in the PISCES-B facility in San Diego [24,7] and in earlier simulations of pure Be samples [23]. Other interesting molecules which we found to be sputtered are  $\text{BeD}_2$  and  $\text{CD}_3$ . Overall, very few hydrocarbons and only one methane molecule  $\text{CD}_4$  were observed. As expected, the carbon terminated surface has a larger sputtering yield of carbon than the beryllium terminated surface.

Fig. 2 shows the sputtering yield for the Be-terminated surface and the C-terminated surface. For comparison experimental data is added. The Exp. data 1 in Fig. 2 are ion beam experimental results published in [25] and the Exp. data 2 [7] are from the linear plasma device PISCES-B. In the latter, the sputtering yields were measured for *in situ* plasma-deposited Be layers on C. When these elements come in contact,  $\text{Be}_2\text{C}$  can form. The sputtering data were gathered after the topmost layer consisting of Be had been removed probably leaving behind a  $\text{Be}_2\text{C}$  layer. The sputtering yields of the two experiments (where different samples and different methods have

**Table 1**  
Sputtered molecules during deuterium bombardment of beryllium carbide (Be<sub>2</sub>C).

	D energy (eV)	Be	BeD	BeD <sub>2</sub>	BeD <sub>3</sub>	BeC	C	C <sub>2</sub>	CD	CD <sub>3</sub>	CD <sub>4</sub>	Tot. sput.	No. bomb.
Be-surf.	10	0	0	0	0	0	0	0	0	0	0	0	3200
	15	0	0	0	0	0	0	0	0	0	0	0	4000
	20	0	4	2	1	0	0	0	0	1	0	8	4000
	50	11	14	3	0	1*	0	0	0	0	0	30	4000
	75	15	15	3	0	0	0	0	0	0	0	33	4000
	100	34	16	3	0	0	1	0	0	0	0	54	4000
C-surf.	10	0	0	0	0	0	0	0	0	0	0	0	2400
	15	0	3	1	0	1**	0	0	0	1	1	8	3200
	20	1	4	1	0	0	0	0	0	0	0	6	4000
	50	6	7	1	0	0	0	0	0	2	0	16	4000
	75	15	6	2	0	0	2	1	1	0	0	27	4000
	100	22	6	0	0	1	8	0	1	1	0	40	4000

\* In fact, a BeDCD molecule sputtered.

\*\* In fact, a BeDCD<sub>3</sub> molecule sputtered.

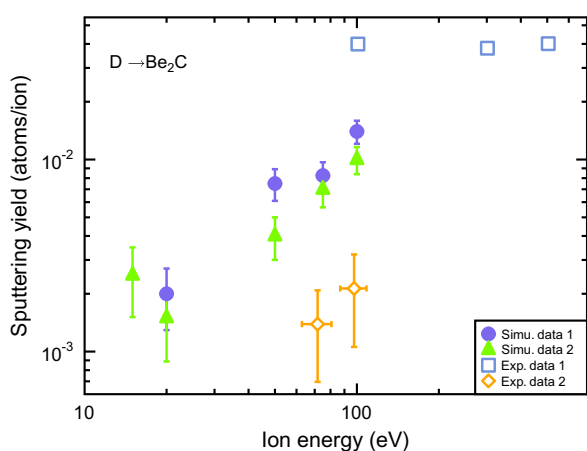


**Fig. 2.** The total sputtering yield (Be+C) of beryllium carbide, Be<sub>2</sub>C. The simulated values are for cumulative D bombardments of both a beryllium (simu. data 1) and a carbon terminated surface (simu. data 2). The Exp. data 1 have been published in [25] and the Exp. data 2 have been published in [7].

been used) differ greatly, something which has been observed in previous studies in pure beryllium as well [7,23,26]. The reason is, however, not clear yet.

As illustrated, the simulation yields are roughly in the same order of magnitude as experimental ones, although straightforward comparison between simulation and the experimental values is however not possible, not only due to the scatter in the experimental data points, but also due to the different fluxes that were used in the simulations vs. experiments. What is more, the sputtering yields may also differ due to the difference in fluences, the MD simulation fluences reached several orders of magnitude lower values to experimental values with steady state sputtering yields obtained by having high fluences [25]. For a discussion on MD sputtering yields fluence dependence compared to steady state see [27].

Fig. 2 illustrates that higher energy bombardment results in a higher sputtering yield. The simulations show that the sputtering from the carbon and beryllium terminated surfaces results in similar yields, with the carbon surface yields being only slightly higher (the reason for which will be discussed in Section 3.3).

### 3.2. ERO modelling: MD sputtering yields implementations

For the plasma impurity modelling, the MD simulation data were fitted with the Bohdansky formula [28]

$$Y(E_0, \alpha = 0^\circ) = Q_n^{\text{KrC}}(\varepsilon) \left(1 - \left(\frac{E_{\text{th}}}{E_0}\right)^{2/3}\right) \left(1 - \frac{E_{\text{th}}}{E_0}\right)^2 \quad (1)$$

for calculating sputtering yields from test particle impacts (with normal incidence) in the ERO code. Here  $Q$  and  $E_{\text{th}}$  (threshold energy where the sputtering yield becomes zero) are fitting parameters that were imported to ERO,  $\varepsilon = E_0/E_{\text{TF}}$ , where  $E_{\text{TF}}$  is the Thomas–Fermi energy, and  $s_n^{\text{KrC}}$  is the nuclear stopping cross section based on the Kr-C potential, given by [8]

$$s_n^{\text{KrC}}(\varepsilon) = \frac{0.5 \ln(1 + 1.2288\varepsilon)}{\varepsilon + 0.1728\sqrt{\varepsilon} + 0.008\varepsilon^{0.1504}} \quad (2)$$

In addition to Be sputtering by D and Be, we also expressed the Be<sub>2</sub>C sputtering using this formula. The resulting values for fitting parameters  $Q$  and  $E_{\text{th}}$  are given in Table 2. For background plasma sputtering, the yields were averaged over the Maxwellian energy distribution and an assumed cosine distribution for the impact angle. Ions are accelerated towards the surface in the plasma sheath; therefore the averaged yields are expressed as functions of the electron temperature separately for each charge state (see Figs. 3 and 4).

### 3.3. The sputtering mechanism, D on Be<sub>2</sub>C

The main sputtering mechanisms have been identified as physical sputtering and swift chemical sputtering (SCS) [29–31,23,32]. Previous MD simulations with deuterium bombardment on pure beryllium surfaces have also identified these to be the main sputtering mechanisms [23]. Figs. 5 and 6 show the ratio of beryllium and carbon sputtered as molecules. The fraction illustrates the significance of either the physical or the SCS process, as single atoms are mostly sputtered by the physical sputtering mechanism and molecules/clusters are mostly sputtered by the SCS mechanism. In the low energy range (15–20 eV) SCS occurred more frequently while for the higher energy ranges (75–100 eV) physical sputtering occurred more frequently.

Fig. 7 shows a single case for SCS on the carbon terminated surface for a Be atom at 15 eV deuterium bombardment. The pictures (a)–(f) are snapshots from the sputtering process at the indicated times in the energy graph, which illustrates the kinetic energy of the incoming D ion and the change in potential energy of the atom that is to be sputtered as well as its initial neighbours. The kinetic

**Table 2**  
Fitting parameters for the Bohdansky formula, Eq. (1).

	Old		New	
	$Q$	$E_{\text{th}}$	$Q$	$E_{\text{th}}$
D on Be	0.11	13.09	0.0671	4.09
Be on Be	0.67	24.17	0.3450	17.83
D on Be <sub>2</sub> C	–	–	0.0526	11.58

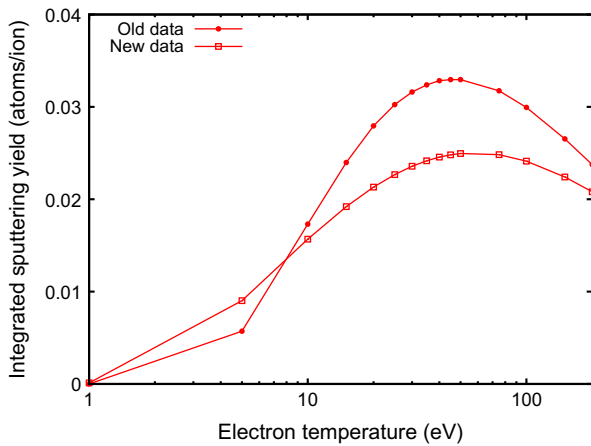


**Fig. 3.** Average sputtering yield of plasma deuterium ions on beryllium surface as a function of electron temperature. It is assumed that the energy distribution is a sheath-accelerated Maxwellian and that the impact angle cosine is evenly distributed.

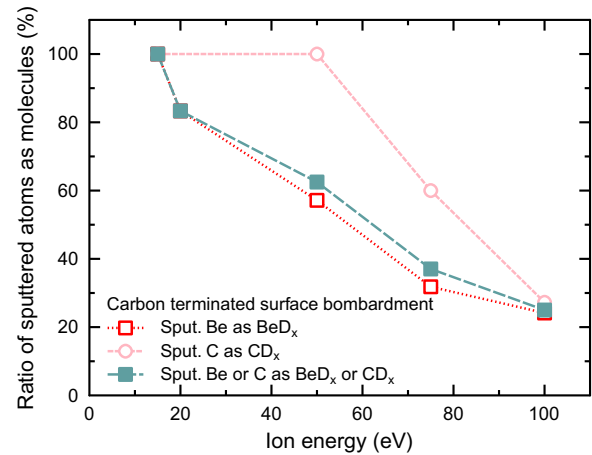


**Fig. 6.** The fraction of beryllium and carbon atoms sputtered as molecules at different energies for the carbon terminated surface simulations.

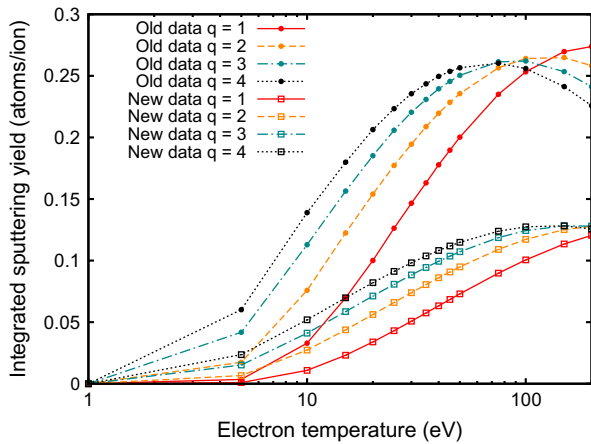


**Fig. 4.** Average sputtering yield of different charge states  $q$  of plasma impurity beryllium ions on beryllium surface as a function of electron temperature. It is assumed that the energy distribution is a sheath-accelerated Maxwellian and that the impact angle cosine is evenly distributed.

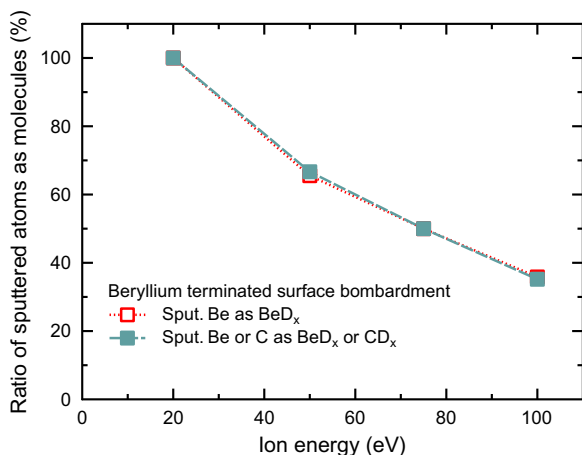


**Fig. 5.** The fraction of beryllium atoms sputtered as molecules at different energies for the beryllium terminated surface simulations.

energy of the D ion drops three times indicating collisions with substrate atoms and at each kinetic energy loss there is a

corresponding potential energy gain. As the bombarding deuterium ion loses almost all of its kinetic energy it bounds with a nearby atom, which is seen in the graph as a flattening of the kinetic energy curve. Meanwhile, bonds to the surface are broken and a Be and one of its D neighbours escape as a sputtered BeD molecule.

As mentioned above, SCS occurred mostly at the lower energies (15–20 eV), probably due to the high deuterium contamination within the near-surface layers of the material. This changed the surface structure from the antifluorite structure to a mixture of D, Be, and C with a large deuterium concentration. Similar surface composition change occurred for the pure beryllium case [23]. This means that the surface Be atoms have many bonds to D atoms and fewer bonds to other Be or C atoms, thus requiring much less energy to be released from the surface than would be the case for a perfect surface.

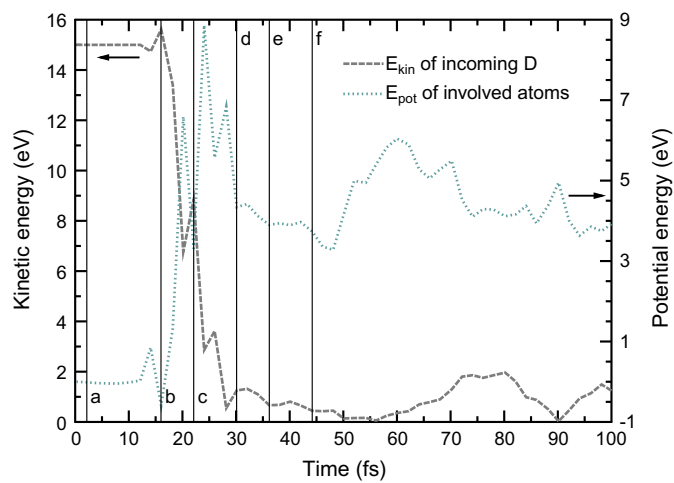
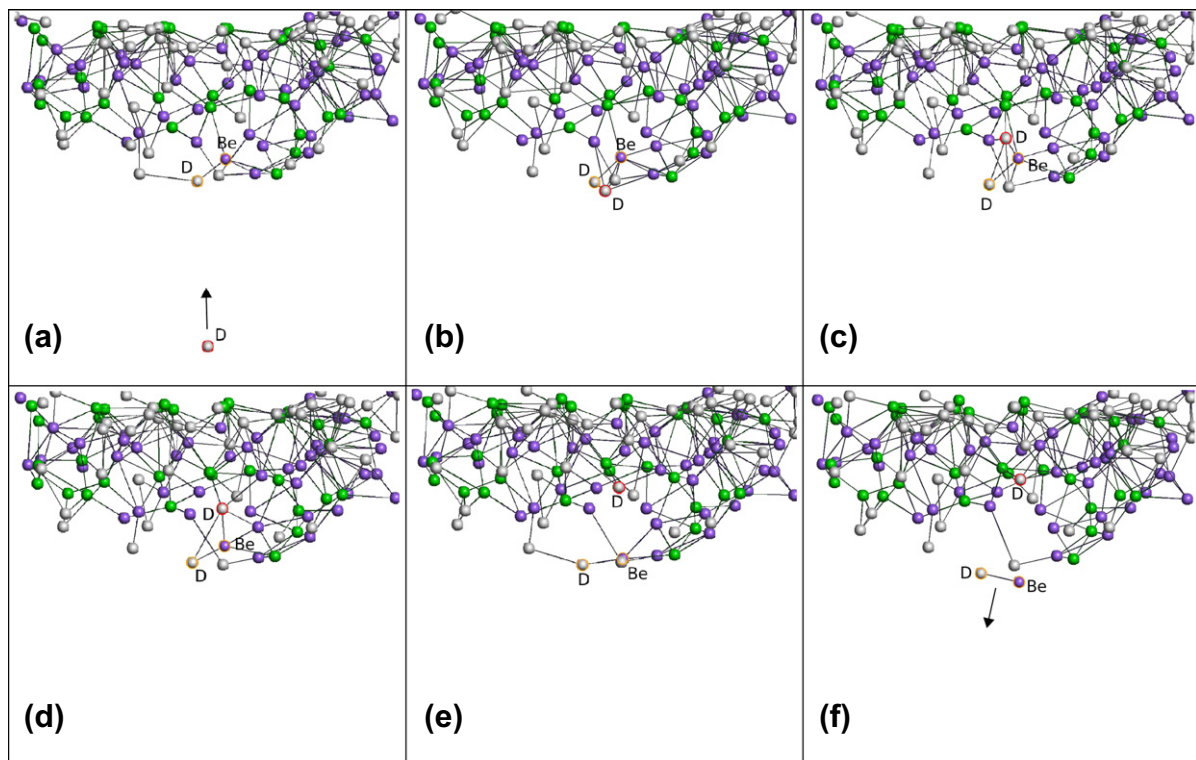
For the higher energy bombardment cases, where mostly physical sputtering occurred, a transformation from an ordered antifluorite structure to an amorphous Be–C–D mixture also took place, but due to the lower deuterium concentration at the surface the chemical sputtering mechanism was not as effective as in the lower energy cases. Also, a higher velocity of an incoming ion makes bond-breaking less probable due to ineffective momentum transfer [30].

Fig. 8 shows the ratio of sputtered carbon atoms versus sputtered beryllium atoms for the carbon terminated surfaces. It is evident that more Be than C atoms sputter even though most sputtered Be or C originated from the topmost surface which was originally made of carbon. Especially for the higher energies beryllium sputters more easily than carbon because of its lower mass.

At lower energies (15–20 eV) the ratio of sputtered C atoms to Be atoms is also low probably because that there were twice as many Be than C atoms in the sample and consequently also in the surface layers. The peak in the carbon sputtering yield at 15 eV is due to one CD<sub>3</sub> and one CD<sub>4</sub> molecule that were sputtered early (during the first 800 bombardments) when the surface still consisted mainly of carbon. Nevertheless, these events show that D ions of only 15 eV are capable of eroding both Be and C.

Interestingly, there was no sputtering at 15 eV for the beryllium terminated surface as opposed to the carbon terminated surface where both beryllium and carbon atoms were sputtered. This indicates that 15 eV is very close to the sputtering threshold. Furthermore, no sputtering occurred for any surfaces at 10 eV indicating that the threshold lies between 10 and 15 eV.

The sputtered atoms were loosely bound surface atoms, which easily break loose by the SCS mechanism. This is seen in Fig. 9 which illustrates the number and type of initial neighbours of



**Fig. 7.** A visualization of the swift chemical sputtering mechanism. The pictures (a)–(f) show how the bombarding deuterium ion (white spheres) break the soon to be sputtered Be atom (blue spheres) bond with its closest carbon atom (green spheres). These pictures are accompanied by an energy graph, illustrating the potential energy changes for the sputtered Be atom and its neighbouring atoms (dotted line) as well as the changes in the kinetic energy of the bombarding deuterium ion (dashed line). The initial potential energy is defined as 0 eV. The pictures are snapshots at the (a)–(f) times indicated in the energy graph. The arrow in picture (f) indicates the final direction of the sputtered molecules. (For interpretation of the references to colour in this figure legend, the reader is referred to the web version of this article.)

the sputtered atoms. At low bombarding energies, 15 and 20 eV, the sputtered atoms have many deuterium neighbours and are more probable to be sputtered.

### 3.4. Blistering

In the 75 eV beryllium terminated surface simulation, a bubble of deuterium was formed inside the cell. Eventually, the bubble grew large enough to separate the topmost layer from the rest of the cell causing one fourth of the cell to be sputtered. This did only occur for 1 of the 12 simulations, however, it significantly increased the sputtering yield from 0.008 to approximately 0.25 and as such is worth to further investigate. This might be an artefact of the high deuterium flux that was used and/or due to not

allowing for thermal migration because of the short time scale in the simulations. Similar blistering/flaking effects have also been observed in WC [33].

### 3.5. ERO results

Fig. 10 shows how the beryllium content of the simulated target area evolves in time in the different ERO simulation cases. A general observation is that the new (pure Be) data set, case 1, decreases accumulation of Be (by increasing sputtering) whereas the new Be<sub>2</sub>C model, case 2, has an opposite effect. Applied simultaneously, the Be<sub>2</sub>C model to some extent overrides the effect of the new data. Fig. 11 shows the surface concentration profile of Be along the outer target after 15 s of plasma exposure in different

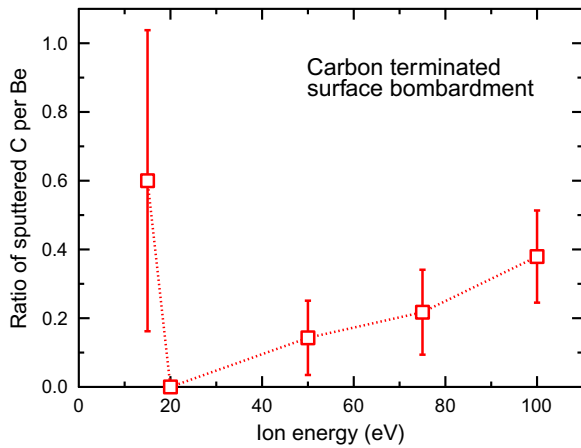


Fig. 8. The ratio of sputtered carbon atoms over the sputtered beryllium atoms at different energies for the carbon terminated surface.

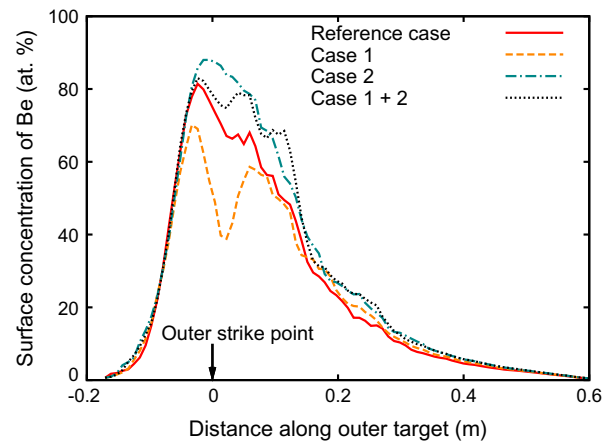


Fig. 11. Surface concentration profile of Be along outer target after 15 s in different ERO simulation cases.

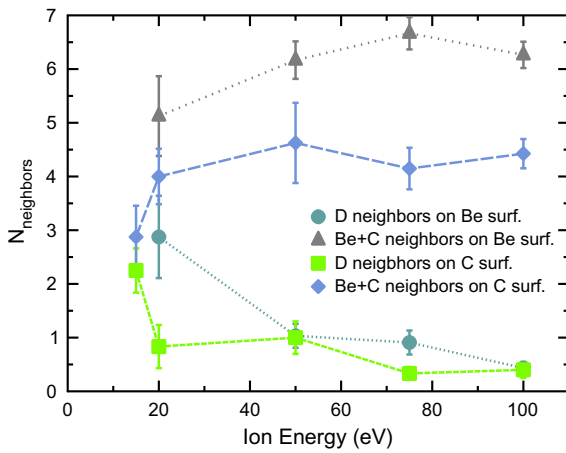


Fig. 9. The average number and type of initial neighbours for the sputtered Be and C. Data for both Be and the C terminated surfaces are shown.

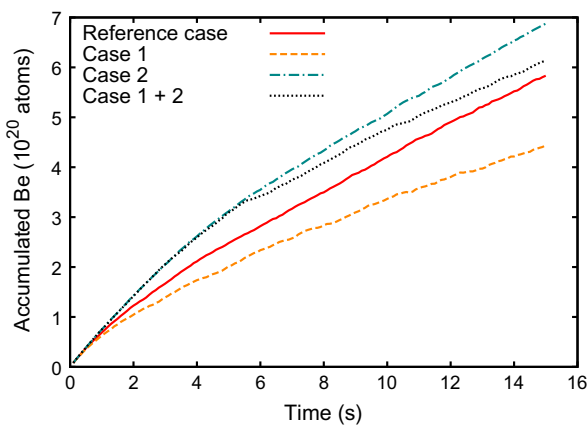


Fig. 10. Accumulation of beryllium onto the simulated outer target area in different simulation cases.

ERO simulation cases. In case 1, the importance of MD data for outer strike point erosion is evidenced by a notable reduction in beryllium accumulation around the strike point.

MD simulations predict generally lower sputtering than the TRIM data used in ERO. For Be on Be, the MD data are systematically lower than TRIM data. Also the new Be<sub>2</sub>C model

suppresses sputtering of both Be and C in comparison to the HMM model. However, Be sputtering by D from pure Be in the low-energy range ( $T_e < 8$  eV for the energy-angle-averaged data) is enhanced as shown in Fig. 3. Because of the target plasma conditions and strong peaking of the particle flux at the outer strike point, this effect is the dominant one in ITER divertor. The electron temperature at the target is about 1 eV in the private-flux region and about 15 eV in the far scrape-off-layer, with a rather steep gradient over a distance about 10 cm, see Fig. 1 of [13].

#### 4. Conclusions

This work describes the sputtering of beryllium carbide Be<sub>2</sub>C by identifying the underlying sputtering mechanisms to be both physical and swift chemical sputtering. It is shown that molecules such as BeD, BeD<sub>2</sub>, and hydrocarbons are sputtered. Furthermore, the results agree quantitatively with the existing, although very scattered, experimental data. More exhaustive experimental confirmation is, however, needed for thorough comparisons.

The threshold for sputtering was determined to lie between 10 and 15 eV. This is a lower thresholds predicted by only considering physical sputtering and implies shorter fusion reactor lifetimes. Both beryllium and carbon atoms are sputtered, though beryllium is seen to sputter preferentially. With ITER in mind, more beryllium than carbon sputtering increases the efficiency as less heat is needed to compensate for the impurity plasma cooling effect.

A high flux of deuterium, like the ones used in the simulations,  $1.88 \times 10^{28} \text{ m}^{-2} \text{ s}^{-1}$ , may lead to deuterium bubble formation and bursting, causing significant sputtering. This might be due to the short simulation time not allowing migration.

This work is a step further in a theoretical understanding of the erosion of mixed materials formed in ITER. It adds to the plasma impurity code ERO an improved surface model that can be later augmented with data for other compounds/mixtures in the Be/C/W system. The sputtering yields obtained in MD simulations were used in plasma impurity simulations for the outer divertor of ITER. With new data for pure Be sputtering and/or with the new Be<sub>2</sub>C model the accumulation rate of impurity beryllium from plasma to the divertor target changes within a  $\pm 25\%$  range compared to the estimate given in [13]. Such changes are modest in the view that the tritium retention rate based on this estimate increased by about 50% in the update given in [34]. Extension of the data set to the full ITER material mix will be reported in a subsequent paper.

## Acknowledgments

This work was supported by EURATOM-Tekes and carried out within the framework of the European Fusion Development Agreement. The views and opinions expressed herein do not necessarily reflect those of the European Commission. The work was partially funded by the Academy of Finland SimITER project. Computing resources have been provided by CSC, the Finnish IT Centre for Science. CSC is owned by the Ministry of Education. The ERO code package is developed by Forschungszentrum Jülich, Institut für Energieforschung – Plasmaphysik.

## References

- [1] C. Linsmeier, J. Luthin, P. Goldstrass, Mixed material formation and erosion, *Journal of Nuclear Materials* 290–293 (2001) 25–32.
- [2] R.P. Doerner, The implications of mixed-material plasma-facing surfaces in ITER, *Journal of Nuclear Materials* 363–365 (2007) 32–40.
- [3] H. Bolt, V. Barabash, G. Federici, J. Linke, A. Loarte, J. Roth, K. Sato, Plasma facing and high heat flux materials – needs for ITER and beyond, *Journal of Nuclear Materials* 307–311 (2002) 43–52.
- [4] The ITER Organization <<http://www.iter.org/>>.
- [5] J. Roth, E. Tsitrone, A. Loarte, T. Loarer, G. Counsell, R. Neu, V. Philipps, S. Brezinsek, M. Lehnen, P. Coad, C. Grisolia, K. Schmid, K. Krieger, A. Kallenbach, B. Lipschultz, R. Doerner, R. Causey, V. Alimov, W. Shu, O. Ogorodnikova, A. Kirschner, G. Federici, A. Kukushkin, Recent analysis of key plasma wall interactions issues for ITER, *Journal of Nuclear Materials* 390–391 (2009) 1.
- [6] R.P. Doerner, M. Baldwin, J. Hanna, C. Linsmeier, D. Nishijima, R. Pugno, J. Roth, K. Schmid, A. Wiltner, Interaction of beryllium containing plasma with ITER materials, *Physica Scripta* T128 (2007) 115–120.
- [7] D. Nishijima, R. Doerner, M.J. Baldwin, G. De Temmerman, Erosion yields of deposited beryllium layers, *Journal of Nuclear Materials* 390–391 (2009) 681.
- [8] U. Kögler, J. Winter, 3D-Monte-Carlo code for local impurity-modeling in the scrape-off layer of TEXTOR, version 2.0, Tech. rep., Forschungszentrum Jülich, 1997.
- [9] A. Kirschner, V. Philipps, J. Winter, U. Kögler, Simulation of the plasma-wall interaction in a tokamak with the Monte Carlo code ERO-TEXTOR, *Nuclear Fusion* 40 (2000) 989.
- [10] A. Kirschner, P. Wienhold, V. Philipps, J.P. Coad, A. Huber, U. Samm, JET EFDA Contributors, Modelling of carbon transport in fusion devices: evidence of enhanced re-erosion of in-situ redeposited carbon, *Journal of Nuclear Materials* 328 (2004) 62.
- [11] L. Aho-Mantila, M. Wischmeier, D. Coster, M. Groth, A. Kirschner, K. Krieger, H.W. Müller, V. Rohde, R.L. Neu, S. Potzel, B. Sieglin, E. Wolfrum, The ASDEX upgrade team, effect of ExB driven transport on the deposition of carbon in the outer divertor of ASDEX Upgrade, *Journal of Nuclear Materials*, in press. <[http://www.sciencedirect.com/science?\\_ob=ArticleURL&udi=B6TXN-51GRW-MS-2&\\_user=949111&\\_coverDate=11%2F17%2F2010&\\_rdoc=1&\\_fmt=high&\\_orig=gateway&\\_origin=gateway&\\_sort=d&\\_docanchor=&view=c&\\_acct=C000049116&\\_version=1&\\_urlVersion=0&\\_userid=949111&md5=2b5d179b86106d9967f1264467fa74ee&searchtype=a](http://www.sciencedirect.com/science?_ob=ArticleURL&udi=B6TXN-51GRW-MS-2&_user=949111&_coverDate=11%2F17%2F2010&_rdoc=1&_fmt=high&_orig=gateway&_origin=gateway&_sort=d&_docanchor=&view=c&_acct=C000049116&_version=1&_urlVersion=0&_userid=949111&md5=2b5d179b86106d9967f1264467fa74ee&searchtype=a)>.
- [12] M.I. Airila, L. Aho-Mantila, S. Brezinsek, J.P. Coad, A. Kirschner, J. Likonen, D. Matveev, M. Rubel, J.D. Strachan, A. Widdowson, S. Wiesen, JET EFDA Contributors, ERO modelling of local deposition of injected <sup>13</sup>C tracer at the outer divertor of JET, *Physica Scripta* T138 (2009) 014021.
- [13] A. Kirschner, D. Borodin, S. Droste, V. Philipps, U. Samm, G. Federici, A. Kukushkin, A. Loarte, Modelling of tritium retention and target lifetime of the ITER divertor using the ERO code, *Journal of Nuclear Materials* 363–365 (2007) 91.
- [14] D. Borodin, A. Kirschner, A. Kreter, V. Philipps, A. Pospieszczyk, R. Ding, R. Doerner, D. Nishijima, J. Yu, Modelling of Be transport in PSI experiments at PISCES-B, *Journal of Nuclear Materials* 390–391 (2009) 106.
- [15] D. Naujoks, W. Bohmeyer, A. Markin, I. Arkipov, P. Carl, B. Koch, H.-D. Reiner, D. Schröder, G. Fussmann, Transport and deposition of hydrocarbons in the plasma generator PSI-2, *Physica Scripta* 111 (2004) 80.
- [16] W. Eckstein, C. Garcia-Rosales, J. Roth, W. Ottenberger, Sputtering data, Tech. rep., Max-Planck-Institut für Plasmaphysik, 1993.
- [17] K. Nordlund, PARCAS computer code. The main principles of the molecular dynamics algorithms are presented in [35,36]. The adaptive time step and electronic stopping algorithms are the same as in [37] (2006).
- [18] C. Björkas, N. Juslin, H. Timko, K. Vörtler, K. Nordlund, K. Henriksson, P. Erhart, Interatomic potentials for the Be–C–H system, *Journal of Physics: Condensed Matter* 21 (2009) 445002.
- [19] H.J.C. Berendsen, J. Postma, W. van Gunsteren, A. DiNola, J. Haak, Molecular dynamics with coupling to an external bath, *Journal of Chemical Physics* 81 (8) (1984) 3684–3690.
- [20] J.F. Ziegler, J.P. Biersack, U. Littmark, *The Stopping and Range of Ions in Matter*, Pergamon, New York, 1985.
- [21] B.S. Mitchell, *An Introduction to Materials Engineering and Science: For Chemical and Materials Engineers*, John Wiley & Sons, Hoboken, New Jersey, USA, 2008.
- [22] D.A. Porter, K.E. Easterling, *Phase Transformations in Metals and Alloys*, Nelson Thornes, Cheltenham, United Kingdom, 2001.
- [23] C. Björkas, K. Vörtler, K. Nordlund, D. Nishijima, R. Doerner, Chemical sputtering of Be due to D bombardment, *New Journal of Physics* 11 (2009) 123017.
- [24] D. Nishijima, R. Doerner, M.J. Baldwin, G. De Temmerman, E.M. Hollmann, Properties of BeD molecules in edge plasma relevant conditions, *Plasma Physics and Controlled Fusion* 50 (2008) 125007.
- [25] E. Gauthier, W. Eckstein, J. Laszlo, J. Roth, Physical sputtering of low-Z materials, *Journal of Nuclear Materials* 176 & 177 (1990) 438–444.
- [26] J. Roth, W. Eckstein, M. Guseva, Erosion of Be as plasma-facing material, *Fusion Engineering and Design* 37 (1997) 465–480.
- [27] K. Vörtler, C. Björkas, K. Nordlund, The effect of plasma impurities on the sputtering of tungsten carbide, *Journal of Applied Physics Condensed Matter* 23 (2011) 085002. <<http://stacks.iop.org/0953-8984/23/8/085002>>.
- [28] J. Bohdansky, A universal relation for the sputtering yield of monatomic solids at normal ion incidence, *Nuclear Instruments and Methods in Physics Research Section B* 2 (1984) 587.
- [29] E. Salonen, K. Nordlund, J. Keinonen, C.H. Wu, Swift chemical sputtering of amorphous hydrogenated carbon, *Physical Review B* 63 (2001) 195415.
- [30] K. Nordlund, E. Salonen, A.V. Krasheninnikov, J. Keinonen, Swift chemical sputtering of covalently bonded materials, *Pure and Applied Chemistry* 78 (6) (2006) 1203–1212.
- [31] R. Behrisch, W. Eckstein (Eds.), *Sputtering by Particle Bombardment: Experiments and Computer Calculations from Threshold to MeV Energies*, Springer, Berlin, 2007.
- [32] A. Krasheninnikov, K. Nordlund, E. Salonen, J. Keinonen, C. Wu, Sputtering of amorphous hydrogenated carbon by hyperthermal ions as studied by tight-binding molecular dynamics, *Computational Materials Science* 25 (2002) 427–434.
- [33] K. Vörtler, K. Nordlund, Molecular dynamics simulations of deuterium trapping and re-emission in tungsten, *Journal of Physical Chemistry C* 114 (2010) 5382–5390.
- [34] A. Kirschner, D. Borodin, V. Philipps, U. Samm, R. Ding, K. Schmid, J. Roth, A. Kukushkin, G. Federici, A. Loarte, Estimations of erosion fluxes, material deposition and tritium retention in the divertor of ITER, *Journal of Nuclear Materials* 390–391 (2009) 152.
- [35] K. Nordlund, M. Ghaly, R.S. Averback, M. Caturla, T. Diaz de la Rubia, J. Tarus, Defect production in collision cascades in elemental semiconductors and fcc metals, *Physical Review B* 57 (13) (1998) 7556–7570.
- [36] M. Ghaly, K. Nordlund, R.S. Averback, Molecular dynamics investigations of surface damage produced by keV self-bombardment of solids, *Philosophical Magazine A* 79 (4) (1999) 795.
- [37] K. Nordlund, Molecular dynamics simulation of ion ranges in the 1–100 keV energy range, *Computational Materials Science* 3 (1995) 448.